ACTA METALLURGICA SLOVACA
2022, VOL. 28, NO. 4, 188-196

RESEARCH PAPER

GRAIN SIZE EVOLUTION, MECHANICAL AND CORROSION BEHAVIOUR OF PRECIPITATE STRENGTHENED Cu-Ni ALLOY

Cynthia Chinasa NWAEJU[1,2], Amarachukwu Oriehi EBOH[1], Francis Odikpo EDOZIUNO[2,3],

[1]Department of Mechanical Engineering, Nigeria Maritime University, P.M.B. 1005, Okerenkoko, Delta State, Nigeria.
[2]Department of Metallurgical and Materials Engineering, Nnamdi Azikiwe University, P.M.B. 5025, Awka, Nigeria.
[3]Department of Metallurgical Engineering Technology, Delta State Polytechnic, P.M.B. 1030 Ogwashi-Uku, Nigeria.

*Corresponding author: cynthianwaeju@gmail.com & cynthia.nwaeju@nmu.edu.ng, tel.: +234 806 697 4899

Received: 01.10.2022
Accepted: 17.10.2022

ABSTRACT

The grain size characteristics, mechanical properties, and corrosion resistance of Cu-10Ni alloy heat treated at three different temperatures and times were investigated and compared with the synthesized alloy. Mechanical properties such as ultimate tensile strength (UTS), ductility, hardness, and impact strength were determined in the research work. An optical metallurgical microscope was used to examine the structural properties. ImageJ software was also used to measure the grain size distribution of the alloys. The corrosion behaviour of the produced Cu-10Ni alloys is analyzed by potentiodynamic polarization and Electrochemical Impedance Spectroscopy (EIS). After corrosion testing, the surface morphology of the exposed samples is analyzed by scanning electron microscope (SEM) equipped with energy dispersive spectroscopy. The results indicated that average grain size and level of grain distribution improve mechanical properties and corrosion resistance of Cu-10Ni alloy. The precipitate-strengthened Cu-10Ni alloys had a lower corrosion rate compared to as-cast alloys, and their ultimate tensile strength, ductility, and hardness improved with decreasing average grain size distribution. The non-heat treated Cu-10Ni alloy showed a peak value of corrosion rate and average grain size, but a lower value of mechanical properties. An increase in residual stress follows an increase in grain size distribution, which lowers the strength and increases corrosion rates due to more active sites of activation energy. The surface analysis confirms the presence of a protective film on the exposed alloy surface. The research outcome has enabled the improvement of the mechanical and corrosion properties of Cu-10Ni alloys as a component for marine and automobile applications.

Keywords: Grain size distribution; Cu-10Ni alloy; Ageing temperatures; Corrosion resistance; Mechanical properties; Surface morphology

INTRODUCTION

Microstructural features are important in the properties of materials, hence they play an important role in materials research. In order to use materials, it is vital to understand the links between microstructural characteristics and material properties. Copper-nickel alloy has been listed among precipitate strengthened copper alloys with exceptional strength, corrosion resistance, good electrical and thermal conductivity, and fatigue resistance [1][2][3][4]. Cu-Ni gains high strength and corrosion resistance through precipitation of hard secondary phases upon ageing process [5][6]. Cu-Ni alloy has played an inimitable part in marine engineering and is, therefore, consists of two major types of alloy systems that have been utilized for many decades for heat condensers, tube applications, water supply lines, and desalination equipment. In seawater systems, Cu-30Ni and Cu-10Ni alloy systems have been widely used as piping material [7][8]. The two alloys are commonly used due to their low magnetic permeability and maximum resilient flow rate following their high strength, and remarkable resistance to seawater corrosion and biofouling [8][9]. However, in the wider commercial application of the alloy, Cu-10Ni alloy is mostly used because of the less nickel content that aggregates lower material cost [7]. The fundamental properties of Cu-Ni alloy are largely influenced by the presence of copper and its alloying elements. Copper inherently obviates its components from colonization with marine organisms such as mussels, algae, and lichens barnacles, which directly affect the performance when used for industrial applications. For applications where this effect is undesirable, copper alloys are preferred to non-copper alloys such as stainless steel [8][10].

According to Wihelm [10], alloying materials, concentration, and heat treatment parameters such as temperature, time, and rate of cooling all influence the structure of an alloy. These factors ascertained the worker ability of grains in the structure. The grain size controls the mechanical behaviour of Cu-Ni based alloys [8][9][11]. The precipitation hardening process has been proven to be effective in improving the mechanical properties of Cu-Ni alloys by modifying the structure [12]. The phase morphology and the grain size usually have a significant effect on the mechanical properties of the alloy following the influence of the fabrication and precipitation hardening process [13]. The precipitation sequence of an alloy system is known to be extremely sensitive to temperature and time. Cu-10Ni alloy has been selected in this research, and according to study, it is

commercially produced using synthesis and conventional precipitation hardening method. Copper containing nickel is solution-treated at a temperature below the recrystallization area, then quenched in water before ageing at different temperatures and times. The heat treatment process utilized in this research is concerned with the development of Ni precipitate from the ageing effect within the Cu matrix [14][15].

Grain size determination of an alloy is an important procedure for structural analysis, where certain degree of properties enhancement is established. Grain size is the fundamental structural characteristic that enhances the crystallinity of metals according to their physical and mechanical behaviour [16]. Mechanical properties like UTS, hardness, impact strength, and ductility have been reported to have linear relationship with fine grain size dispersal [17]. Fine grains with small distribution width are said to achieve good mechanical strength [18], while exceptionally low strength is obtained as a result of larger grains [19]. When determining the various morphological features of microstructure, the most essential characteristic of metallic materials is average grain size. Hall [20] and Chapetti [21] stated that average grain size is linked to various materials, see also [22]. Average grain size is obtained from the grain size distribution with its measurable effects on most mechanical properties [17][23][24]. A significant mechanical property required to be made with Cu-Ni alloy materials is the combination of high strength, hardness, ductility, and corrosion resistance. As a result, the structure of the component material is expected to be developed such that it will give a suitable balance of metallic properties. Selecting appropriate synthesis and heat treatment parameters pave-way for a fine and uniform grain size microstructure. Metallurgical procedures can cause grain size distribution to deviate from design specifications. It is therefore highly desired for the characterization of grain size distribution, particularly in a non-destructive manner. Grain boundary character and grain orientation are two characteristics related to grain size distribution and is been altered during the alloy production. For decades, a wide range of processing procedures, including casting, forging, rolling, drawing, and extrusion, have been used along with heat treatment to modify the microstructure and improve the mechanical characteristics of metals used in various applications. The grain size distribution, as well as other parameters, are regulated in order to obtain excellent mechanical properties and corrosion resistance [16][25]. The changes in the passive layer characteristics due to alloy processing techniques, environment, and impurity concentration, microstructural refinement of Cu-Ni alloy can result in a significant improvement in corrosion response [26].

The detailed understanding of the effect of grain size on the corrosion response of materials is less understood. Grain refinement, which leads to higher strength in crystalline materials, is predicted using the classical Hall–Petch relationship [20][27]. The relation suggests that the corrosion rate varies inversely with the square root of the average grain diameter. Srikant [28] proposed a relationship that correlates corrosion rate with grain size distribution. The relationship shows that corrosion behaviour is a function of grain size distribution, and as grain size broadens and increases, the corrosion rate of an alloy decreases in a non-passivating environment, but increases in a passivating environment, and vice versa. As a result, the equation for the relationship is as follows:

$$i_{uc} = A + B(\bar{d})^{-\frac{1}{2}} exp\left(-\frac{9}{8}S_n^2\right) \quad (1.)$$

Where i_{uc} is uniform corrosion density, A and B are constants derived from corrosion studies and a function of grain size in an alloy. The constants are affected by the material's impurity level and the nature of the corrosive environment. $\bar{d}$ is the mean grain size and S_n is the standard deviation.

The diversity in the size of grains distribution has a significant impact on the corrosion rate and mechanical properties of crystalline metals. Nie [29] reported that corrosion rate decreases as the average grain size decreases in the physiological media of the pure iron. Li [30] revealed that grain boundaries get purer as grain size is reduced according to impurity distribution. The impact of grain size on corrosion properties was reviewed by Ralston and Brubillis [26]. The authors summarized that depending on the processing technique and passivation ability of alloy in an environment, alloys could experience decrease or increase in corrosion resistance with the effect of grain refinement. According to studies, when grain size decreases, corrosion rates decrease. The ability of high grain boundary density surfaces to passivate second phase intermetallic particles more readily is often credited with improved corrosion resistance [31][32][33].

The focus of this research is to determine the grain size distribution development and its effect on the mechanical properties and corrosion behaviour of synthesized and precipitate strengthened Cu-10Ni alloy, with the aim of using the outcome to control and alter Cu-Ni alloy properties for industrial applications. The findings are expected to contribute immensely to the growing field of information on the impact of metallurgical fabrication techniques on the microstructure of copper-nickel alloy as a component of marine and automobile materials.

MATERIAL AND METHODS

Material preparation

The materials employed in the study were 99.9% pure copper wire from Cutis Cable Plc Nnewi, which served as the development matrix, and 99.5% pure nickel granules from Cifa laboratories (CIBIS) New Heaven Enugu, which functioned as the principal alloying element. Direct stir casting in a bailout crucible furnace was used to produce the alloy. The two major metals (copper and nickel) were weighed out, and copper wire was first charged into the furnace, heated to a temperature of about 1000ºC, followed by introducing the nickel granules into the melt and continuously stirring until homogeneity is attained. The molten mixture was left for about 10mins to achieve complete dissolution of nickel metal. The melt was poured into a 45x55x155mm^3 pre-heated steel mould in an argon atmosphere. The ingots were homogenized for 5 hours at 600°C after casting before being air cooled to ambient temperature. The ingots were then quenched in cold water after being solution treated for 2 hours at 900ºC. The quenched samples were aged in the furnace for 1 hour and 2 hours at 400ºC, 450ºC, and 500ºC, respectively. The samples were removed from the furnace and allowed to cool spontaneously in the open air.

Structural and grain size analysis

An optical metallurgical microscope (Model: L2003A) was used to examine the structural features of the produced samples. Grinding, polishing, and etching were used to prepare the samples such that the structure could be examined using the metallurgical microscope. The samples were polished with fine alumina powder after being ground with a series of emery papers with grits of 220, 500, 800, and 1200. Before mounting the samples on the microscope for microstructure examination and micrographs, an iron (iii) chloride acid was utilized as an etching agent. The grain analysis, which included determining the average grain size and grain size distribution was carried

out using the linear intercept method of ImageJ software, and the procedure was as described [24][34]. The surface corrosion morphology of the investigated samples was studied using JEOL JSM 7600F scanning electron microscopy (SEM) equipped with energy dispersive X-rays (EDS).

Mechanical test

The mechanical properties were determined by measuring the UTS, ductility, hardness, and impact energy. The tensile test was carried out on an Instron Universal Tester (model 3369), which depicted the measurement of UTS and ductility at a strain rate of 10-3/s in ambient temperature. It was carried out in ASTM B557M standard. A Brinell hardness testing machine (model 900-355) was used to determine the hardness of the produced samples. A Charpy machine type IT-30 was used to test the alloy's impact strength on notch samples. For the impact test, the samples were machined at 55x10x5mm^3 with a 2mm deep notch at a 45^o angle and a radius of 0.25mm according to the ASTM F2231 standard. The mechanical results were calculated using an average of at least three specimens.

Electrochemical measurement

The corrosion behaviour of the produced alloy was conducted in as-cast and heat-treated conditions. The test was carried out in neutral seawater of 3.5wt % NaCl solution using Autolab CH1604E electrochemical measurement system. Samples with the size of 1mm ×1mm × 1mm were cut from the alloy ingots for electrochemical tests. As described [35], polarization measurements were performed using a conventional three-electrode Pyrex glass cell. Test specimens with 1mm x 1mm area of exposed areas were used as working electrodes, with a platinum rod serving as the counter electrode for each measurement. A saturated calomel electrode (SCE) was used as the reference electrode, with a luggin probe placed next to the working electrode. All of the investigations were performed in a simulated seawater solution. A stable open circuit potential was achieved by immersing the working electrode in the test solution for 3000s. The corrosion current density (I_{corr}) and the corrosion potential (E_{corr}) were determined using a potentiodynamic polarization study with a linear sweep technique at a scan rate of 1.0 mV/s and a potential range of -150 mV to +150 mV. Each sample's EIS was calculated at a frequency of 100 kHz to 0.1 Hz in the same solution. The corrosion rate was calculated from the Tafel curves using equation (2) and the impedance data was analysed using the EIS spectrum analyser software with impedance system by Barsoukov [36], measuring from frequencies of 0.01Hz and 10^{5}Hz.

$$\boldsymbol{CR} = \frac{\boldsymbol{3.96\,MJ.}}{\boldsymbol{n\rho}} \qquad (2.)$$

Where
CR = corrosion rate
3.96= surface area of the electrode
M = formula molecular weight of the alloy
J = corrosion current density
n = valency/no of electrons
ρ = density of the sample

RESULTS AND DISCUSSION

Microstructural observation

The microstructural characteristics of the observed samples are shown in **Fig. 1a-d**. The microstructures are presented as a function of three variable ageing temperatures (400^{0}C, 450^{0}C, and 500^{0}C) for 2hrs and as-cast.

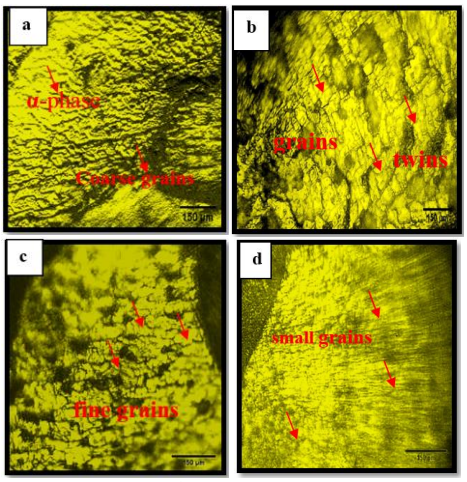

Fig. 1 Microstructure of Cu-10Ni alloys: (a) as cast (b) Aged at 400ºC (c) Aged at 450ºC (d) Aged at 500ºC for 2hr

It was generally observed that the examined microstructures were composed of α-Cu with lots of equiaxed grains with twins. Each of the examined microstructures contains one kind of Ni- containing phase as reported in [37]. In Fig. 1a, a typical dendrite structure was observed with the sample of as-cast Cu-10Ni alloy. The microstructure of the as-cast sample consists of a large, coarse, linked interconnected intermetallic ($Cu_2Ni)_3$ compound in α-phase. The dendritic structure completely disappeared, showing that the alloy has been homogenized and solution treated [38]. Fig 1b-d shows the microstructure of homogenized and aged alloy specimens. The microstructure of the Cu-10Ni alloy at different ageing temperatures revealed homogenous recrystallized fine grains with many twins. The twins have a Ni-rich -phase with an orthorhombic structure, which differs from the non-heat treated Cu-10Ni alloy. The ageing process resulted in the formation of fine α-phases and Cu_4Ni_2 intermetallic particles (see Fig 1b-d). During the ageing process, clustering in terms of phase separation and ordering reaction takes place, and the Ni atoms precipitate as Ni_2 and Ni_3 [4][39]. Precipitates act as impediments to the movement of dislocations during deformation [5]. As a result, the precipitation hardening mechanism effectively strengthened the alloy. As depicted in Fig. 1b-d, ageing at different temperatures refines grain size and increases the nucleation rate of the precipitates. The Cu-Ni alloy can thus acquire exceptional mechanical properties. The ageing precipitates referentially dissolve during the electrochemical corrosion test because they have an anodic potential in comparison to the copper matrix [40]. Increasing ageing temperatures cause precipitates to grow in size and form along the grain boundaries. Hence, Figs. 1c and 1d show that after ageing at 450ºC and 500ºC for 2 hrs, a visible amount of fine second phase particles precipitate in the copper matrix, leading to complete filling of the grains along the grain boundaries.

Grain size evolution

By measuring the grains in the microstructure, the grain size distribution was determined. The threshold, an important tool in ImageJ software, was used to measure the distance between

grains and grain boundaries. Threshold detects both grain boundaries with the grain interior in order to find the average grain size of an alloy [41]. In Fig. 2a-d, generated threshold micrographs, the orientation difference in grain distribution of each of the maps and the fitting model of the grain diameter distribution can be observed. The synthesis and precipitation-hardening processes alter the grain size distribution of Cu-10Ni, as shown in Fig. 2. After ageing, Cu-10Ni alloys showed decreased broader grain size distribution and mean recrystallized grain sizes in their variable temperature. In comparison to the threshold image of the generated aged Cu-10Ni alloys, the threshold map of the as-cast sample comprised enormous coarse equiaxed grains, as seen in Fig.2a. The α-phase was observed not to be well dispersed within the matrix, hence, large and equiaxed grains were not identified. The average grain size measured from the as-cast alloy is ≈ 65.54 ± 12.28μm with a total grain count of 785 and a maximum diameter of 36.124m. The grain boundary distribution is visible in Figs 2b-d. Different state of grains was indicated as the grain size varies with the ageing temperature.

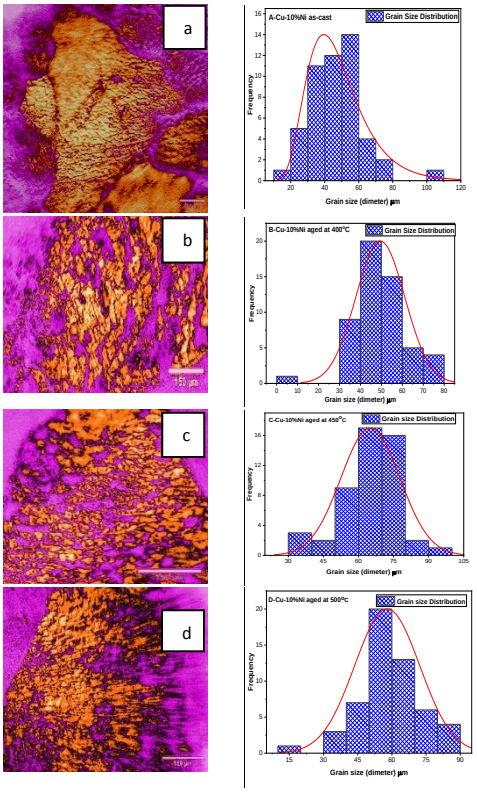

Fig. 2 Grain colour orientation map and grain distribution of Cu-10Ni alloys: (a) as cast (b) Aged at 400ºC (c) Aged at 450ºC (d) Aged at 500ºC for 2hr

The grain orientation maps were observed to have a typical coffee beam contrast of semi-coherent spherical grains, with no distorted grains dispersed throughout. The calculated average grain size of the aged alloy is ≈ 49.49±11.70μm-Cu-10Ni at 400^0C, ≈43.50 ± 12.07μm-Cu-10Ni at 450^0C, and ≈ 42.92 ± 14.28μm -Cu-10Ni at 500^0C. At the 978grain count measurement, the grain size varies from less than 16μm. The decrease in average grain size shows that the properties of the Cu-10Ni alloy were improved [41][42]. Small grains have a higher grain boundary density than large grains in the same space. They are more receptive to enhancing alloy properties. As can be deduced from their evolution, both the mean grain size and the distribution width values grew rapidly during the ageing process. Because of the variance in grain diameter distribution, the grain orientation map (**Fig.2**) reveals that there is morphological grain size difference between the as-cast and aged samples. The aged samples have been strengthened, resulting in a uniform and fine precipitates. The grain data distribution was well-fitted by a log-normal function of the statistical scale presented as a solid line. A log-normal function depicts that grain structure is mainly poised of small grains completed by larger grains [41][43].

Mechanical properties and grain effect

The results of the mechanical testing of the samples are shown in Figures 4–7. Mechanical properties such UTS, ductility, hardness, and impact energy were evaluated in this research. Fig. 3 shows the comparison of the stress-strain curve that gave the tensile characteristics. It was observed generally that the evaluated mechanical properties of as-cast Cu-10Ni alloy have lesser improvement than the heat-treated samples. The trend of performance of the tensile properties was represented through the stress-strain curve. A progressive increase was observed with the aged samples in **Fig. 3**. **Figs. 4–6** show that increasing the ageing temperature and holding duration increased UTS, ductility, and hardness. At the ageing condition of 500ºC for 2hr, the

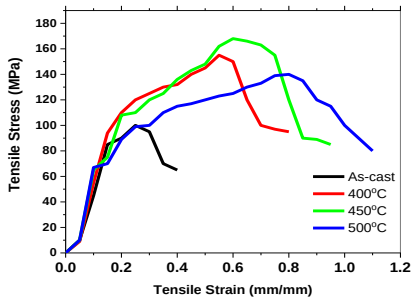

Fig. 3 Tensile stress-strain curves of Cu-10Ni alloy

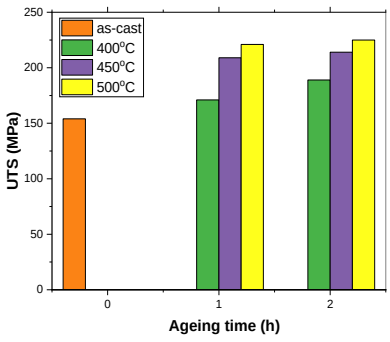

Fig. 4 UTS of Cu-10Ni alloy aged at different temperatures and time

peak values of the aforementioned mechanical properties were obtained. The optimum values of UTS, ductility, and hardness are 225MPa, 15.4%, and 134.8HBN, respectively. These values are higher than those obtained from as-cast samples. It is worth noting that the parameters used in the ageing process have a significant impact on the enhancement of alloy properties, which is consistent with Wihelm's literature report [10]. The impact strength result is presented in **Fig 7**. The impact strength of all

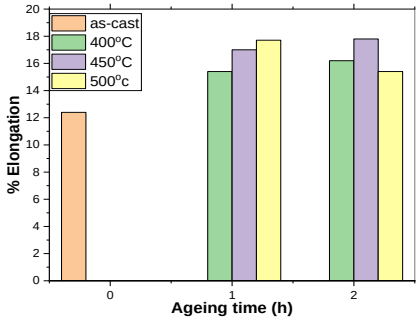

Fig. 5 %Elongation of Cu-10Ni alloy aged at different temperatures and time

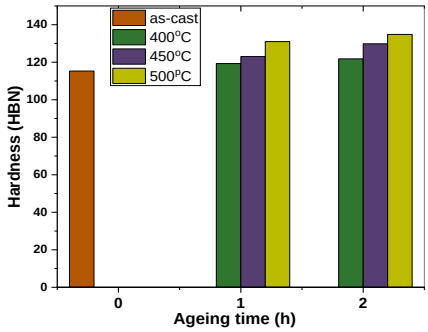

Fig. 6 Hardness of Cu-10Ni alloy aged at different temperatures and time

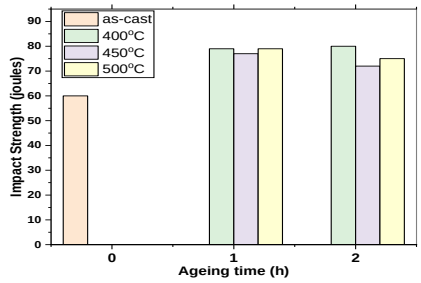

Fig. 7 Impact strength of Cu-10Ni alloy aged at different temperatures and time

the tested samples was observed to decrease as the ageing temperature and time increased, implying that the process parameter did not affect the ability of alloy to absorb energy before fracture will occur. The enhancement in the mechanical properties of aged samples can be ascribed to the decrease in broader grain size distribution. Precipitates produced in the matrix by the ageing process efficiently inhibited dislocation movement, allowing an alloy to pave the way for the improvement of properties. When compared to the as-cast Cu-10Ni alloy, the average grain size of the aged samples decreases, and the particles are smaller and more evenly distributed. The sensitivity of strain rate of an alloy is affected by grain size distribution which therefore helps to attain uniform distribution of grains in the alloy matrix interface [16][41]. This process contributes significantly to the improvement of mechanical properties.

Corrosion behaviour and grain size effect
Potentiodynamic polarization characterization

The potentiodynamic polarization curves for Cu-10% Ni alloy in as-cast and aged conditions produced in 3.5wt% NaCl solution are presented in **Fig. 8**. The parameters in Fig. 8 were calculated and tabulated in **Table 1**, including E_{Corr}, I_{Corr}, cathodic (B_c) and anodic (B_a) Tafel slopes, polarization resistance (R_P), and corrosion rate (CR). The tested specimens showed similar polarization and passivity characteristics under all conditions. However, the corrosion current densities (I_{corr}) and corrosion potentials (E_{corr}) of the as-cast and aged alloys

Table 1 Polarization parameters and rates of corrosion of as-cast and aged Cu-10Ni alloys in 3.5wt% NaCl solutions

Specimens	Electrochemical Parameters Associated with Polarization Measur					
	I_{corr} (μA/cm)	E_{corr} (V_{SCE})	R_p (Ωcm^2)	B_c (V.dec)	B_a (V.dec)	CR (mpy)
As-cast	1.172	-0.676	214.4	5.771	11.528	14.057
Aged at 400°C	3.111	-0.835	252.7	6.672	2.484	11.057
Aged at 450°C	2.188	-0.583	297.7	3.786	6.263	7.838
Aged at 500°C	1.445	-0.583	359.3	1.204	7.163	8.534

I_{corr} = Corrosion density, E_{corr} = Corrosion potential, B_c = cathodic tafel slope, B_a= anodic tafel slope, CR = Corrosion rate, R_p = Linear polarization resistance.

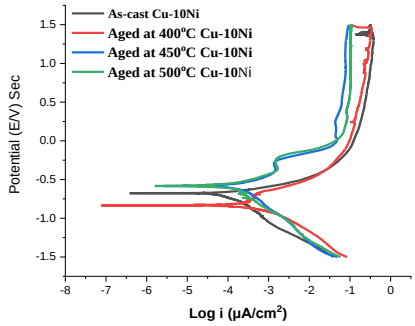

Fig. 8 Potentiodynamic polarization curves of as-cast and aged Cu-10Ni alloys in 3.5wt% NaCl solutions

show considerable differences in corrosion rates. The potentiodynamic curves for the 3000s corrosion measurement revealed a continuous shift in corrosion potential (E_{corr}) towards less negative values, indicating that there is increasing passivation. The level of the positive shift was recorded more with aged Cu-10Ni alloy. It can be noted that the susceptibility to corrosion is measured by corrosion potential and a positive

shift indicates corrosion protection [43]. It is observed in Table 1 that the corrosion current densities were more intense for the as-cast Cu-10Ni alloy. When the value of corrosion density is lower, the corrosion process becomes slower, which shows more corrosion resistance. The polarization resistance (R_p) increased with immersion time and ageing temperature. After 3000s of immersion, the polarization resistance of the aged specimens increased from 252.7cm^2 to 359.3cm^2. The polarization resistance of the as-cast specimen was 214.4 cm^2, which is lower than that of the aged specimen. Polarization resistance is a response to corrosion resistance. The corrosion process is accelerated by residual stress, solute atoms, and lattice distortion [4] [41] [43]. The matrix of the aged sample contains fewer solute atoms, lower residual stress, and smaller lattice distortion than the as-cast sample. Therefore, the aged sample outperforms the as-cast sample in terms of corrosion resistance. **Table 1** shows the corrosion rate of each sample, with the results visible in the Tafel plot. The maximum corrosion rate for the as-cast sample is 14.057mpy, while the minimum corrosion rates for the aged samples are 11.057mpy, 7.838mpy, and 8.534mpy, respectively. The difference in the corrosion rate is attributed to grain refinement, as revealed by the cathodic and anodic kinetics and Tafel curve profiles. The processing technique method of the Cu-10Ni alloy has a significant impact on the alloy grain size [41].

Electrochemical impedance characterization

To evaluate the electrode reactions at the metal/electrolyte interphase and the formation of corrosion products, EIS measurements were carried out in an aerated 3.5wt% NaCl solution. **Fig. 9** shows the impedance spectra as displayed in the form of a Nyquist and a Bode plot. The two capacitive loops linked to two-time constants are clearly visible in the usual Nyquist plots measured on the analysed specimens (Fig 9a). At higher frequencies, Nyquist plots revealed a single semicircle, and at lower frequencies, a diffusive Warburg straight line, showing that the corrosion mechanism is controlled not only by the charge transfer step but also by the diffusion process The time constants are divided into two frequency regions in the high-frequency part, the uncompensated resistance due to the electrolytic solution and the impedance characteristics resulting from the electrolyte penetration through a porous film, and the processes occurring at the substrate/electrolyte interface in the low-frequency part [44]. The Nyquist curves begin with a straight-line path in the low-frequency part that intensifies diffusion impedance characteristics. In the high-frequency part, the impedance characteristics of the resistance solution remained identical and stabilized. The diameter of the semicircle of the Nyquist graph separately increased with the specimen type. The trend is an indication that structural changes occur as a result of grain size distribution. Figs 9b and 9c show the corresponding EIS Bode plots obtained under electrolyte solution. The Bode plots obtained reveal that impedance increases with the immersion time. The Bode plots show that impedance increases as immersion time increases. The investigated samples' Bode plots and phase angle Bode plots revealed similar impedance characteristics. At lower frequencies, as-cast and 400^{0}C aged samples showed similar impedance characteristics, but at higher frequencies, ageing at 450^{0}C and 500^{0}C showed a similar trend, indicating the same corrosion process. Fig. 9b shows the variation of the total impedances of the various samples. The impedance of the sample aged at 400^{0}C shows the lowest values, followed by samples aged at 450^{0}C and 500^{0}C. These values are lower than the as-cast sample. It can be depicted from the Bode phase angle (Fig.9c) that at very high frequency, the phase angle approaches zero, then gradually decreases to lower values in the low-frequency region; the former indicated that solution resistance dominates the impedance in this frequency range, whereas the latter demonstrated the contribution of surface film resistance to the impedance [44]. It's worth noting that while employing the precipitation hardening technique in strengthening Cu–10Ni alloy, the phase maximum shifts to a lower frequency and the phase angle increases to around 80^o. The total impedance increases to a great extent when the alloy is heat treated at three different temperatures.

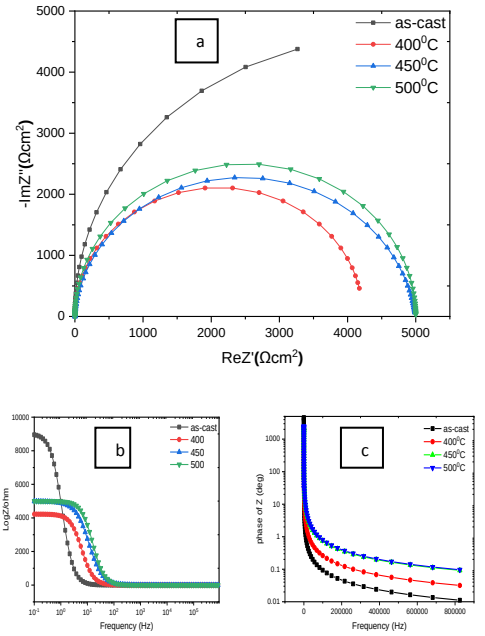

Fig. 9 Impedance spectral of as-cast and aged Cu-10Ni alloys in 3.5wt% NaCl solutions. (a) Nyquist plot (b) Bode plot - impedance, (c) Bode plot- phase angle.

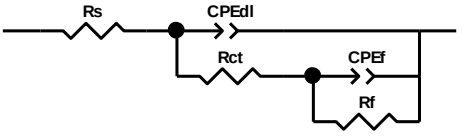

Fig. 10 Equivalent circuit model used to fit experimental impedance data

Table. 2 values of fitted equivalent circuit parameters of Cu-10Ni alloy in as-cast and different ageing temperatures for two hours.

Specimen	R_s (kΩcm^2)	R_f (kΩcm^2)	CPE_{dl} (μF/cm^3)	n_1	CPE_{film} (μF/cm^3)	R_{ct} (kΩcm^2)	n_2
As-cast Cu-10Ni	0.703	0.0301	31.446	1.008	12.448	8.231	1.008
400ºC Aged Cu-10Ni	6.269	0.040	11.524	1.009	12.464	17.54	1.009
450ºC Aged Cu-10Ni	8.493	0.061	24.587	1.10	22.445	18.35	1.10
500ºC Aged Cu-10Ni	11.300	0.058	15.486	1.10	28.152	18. 41	1.10

The impedance spectra were analysed by fitting to the equivalent circuit model shown in **Fig. 10**. From the simple equivalent circuit, the measured data and their best fits are depicted by symbols and solid lines, respectively. The characteristics of the equivalent circuit fitted parameters are listed in **Table 2**. From the established circuit model, R_s represents the resistance solution, R_{ct} represents the charge transfer, R_f is the film resistance, and CPE represents the constant phase element. The electrode impedance from the equivalent circuit, which consists of a parallel combination of constant phase element and resistance charge transfer in series with solution resistance, is represented by equation 3.

$$Z = R_s + \frac{R_{ct}}{1+\{2\pi f R_{ct}+CPE_{dl}\}^{\propto}} \quad (3.)$$

Where $\propto$ indicates an empirical parameter ($0 \leq \propto \leq 1$) and f is the frequency in Hz. The mathematical formula accounts for the distribution of time constants caused by composition inhomogeneities and variations in alloy surface layer [44] [45]. The CPE products describe the process of forming an oxide film on the alloy surface. It is a unique element whose value is determined by an independent function of angular frequency and phase. From the parameters in Table 2, the passive resistance film of R_f of precipitated strengthened Cu-10Ni alloys is higher than that recorded for as-cast alloy. It is an indication that higher corrosion resistance was obtained with heat-treated Cu–10Ni alloys. The recorded high corrosion resistance can be attributed to the uniform passive layer on the alloy surface, which results from the finely dispersed grains of the alloy structure [4]. The values of both R_{ct} and R_s of the aged samples are higher than the as-cast alloy, indicating the formation of a more compact oxide film. It can be deduced from the result that the corrosion resistance of the Cu-10Ni alloy increased with ageing temperature. The observation of the electrochemical impedance parameter has a good agreement with the obtained results of polarization where non-heat treated Cu-10Ni alloy revealed a higher corrosion rate and coarser dendrite of microstructure. The wider semicircle of the Nyquist plot confirms the enhanced corrosion resistance of aged Cu–10Ni alloys [4][42].

SEM and EDX analysis of the corroded surface

The degree of corrosion attack and chemical composition of the corrosion product on the surface of Cu-10Ni alloys at various processing conditions were examined using SEM morphology and its EDX spectra. According to the EDX profile intensity, the corrosion products on the surface layer of the as-cast Cu-10%Ni alloy, revealed in the micrograph of **Fig. 11a**, are most likely a copper oxide variant. The as-cast Cu-10Ni alloy in the sweater (NaCl) solution had a high O-signal intensity as shown by the EDX spectra, signifying the presence of Cu_2O. Cl has been discovered as well, due to chloride precipitation during active dissolution. The surface of the Cu-10Ni matrix is corroded, and the alloy has a considerable defect on the grain boundary as a result of the large grain size distribution. The corrosion attacks in **Fig. 11(b-d)** are barely visible, indicating excellent corrosion resistance. It could be observed from the EDX spectra of the three aged samples that the intensity of the O and Cl signals was significantly reduced. It turned out that Cu-10Ni alloys subjected to the precipitation strengthening process possessed a smoother surface. Discrete grain particles were formed on the surface of the aged specimen depicted by the SEM morphology after immersion for 3000s, and they grew as the ageing temperature increased to 500°C. The particles appeared closely at a smaller the aged specimen depicted by the SEM morphology after immersion for 3000s, and they grew as the ageing temperature increased to 500°C. The particles appeared closely at a smaller size, with a strong protective effect on the specimen. The increase in corrosion products, as the EDX spectra of the varied aged specimen indicated Fe, C, Na, Cl, Al, in reduced intensity, has allowed the corrosion film to become denser, which, as a result, decreases the corrosion rate and increases the corrosion resistance [4][41][44].

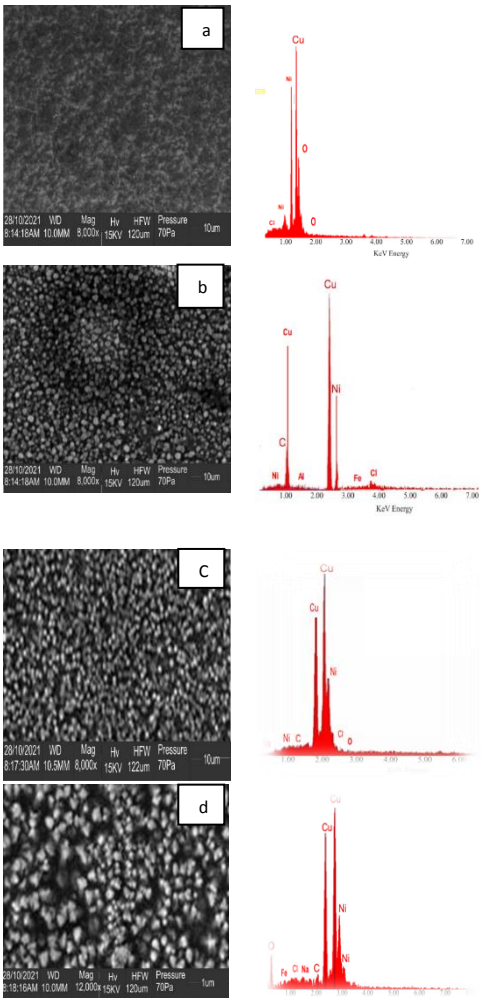

Fig. 11 SEM micrographs with corresponding EDX of the corroded test surfaces of Cu-10Ni alloys after immersion in 3.5wt% NaCl solution (a) as cast (b) Aged at 400°C (c) Aged at 450°C (d) Aged at 500°C

CONCLUSIONS

The grain size evolution and its effect on the mechanical properties and corrosion resistance of a Cu-10Ni alloy has been investigated. The findings reveal that the average grain size and level of grain distribution are functions of the Cu-10Ni alloy in improving mechanical properties and corrosion resistance. The average grain size of the as-cast Cu-10Ni alloy decreased as the

alloy go through the precipitation hardening process. According to the obtained results of this study, the following conclusions can be drawn:

The substantial level of property enhancement displayed by the heat-treated Cu-10Ni alloy shows the linear relationship between the processing technique and grain size distribution. The microstructure constituents of the as-cast Cu-10Ni alloy are large, coarse, linked interconnected intermetallic $(Cu_2Ni)_3$ compounds in α-phase.

1. Grain refinement of the Cu-10Ni alloy achieved through the precipitation hardening process results in an enhancement of mechanical properties and corrosion resistance. The average grain size of the as-cast alloy decreased from 65.54μm to 42.92μm after the ageing process.
2. The mechanical properties (UTS, ductility, and hardness) of Cu-10Ni alloys were observed to improve as the ageing temperature increased with respect to time. The optimum values of UTS, ductility, and hardness were attained at the ageing condition of 500ºC for 2 hours, with values of 225MPa, 15.4%, and 134.8HBN, respectively.
3. In comparing the as-cast and aged Cu-10Ni alloys, the corrosion susceptibility in 3.5wt% NaCl was higher in the as-cast alloy. An increase in average grain size distribution and the presence of coarse grains attribute to the optimum level of corrosion rate of the as-cast alloy. The corrosion rate was found maximum (14.057mpy) in as-cast Cu-10Ni and minimum (7.838mpy) with the alloy aged at 450ºC for 2hrs.
4. The formation of a protective oxide layer is indicated by a higher angle and a larger semicircle in aged samples.
5. The SEM morphological study of all examined aged alloy specimens revealed no apparent corrosion attacks, possibly confirming excellent corrosion resistance under the strengthening conditions.

Acknowledgement: The authors acknowledge the Tertiary Education Trust Fund (TETFund), Nigeria for financially supporting this research through the Institution Based Research (IBR) Interventions.

REFERENCES

1. Lei, Q., Li, Z., Wang, J., Xie, J.M., Chen, X., Li, S., Gao, Y., Li, L.: Hot working behavior of a super high strength Cu–Ni–Si alloy, Materials & Design, 51, 2013, 1104–1109. https://doi.org/10.1016/j.matdes.2013.05.001.

2. Jia, L., Lin, X., Xie, H., Lu, Z., Wang, X.: Abnormal improvement on electrical conductivity of Cu–Ni–Si alloys resulting from semi-solid isothermal treatment, Materials Letters, 77, 2012, 107–109. https://doi.org/10.1016/j.matlet.2012.03.010.

3. Zhang, J., Li, X., Yang, B., Wang, H., Zhang, J.: Effect of micro-shot peening on fatigue properties of precipitate strengthened Cu-Ni-Si alloy in air and in salt atmosphere, Surface and Coatings Technology, 359, 2019, 16–23. https://doi.org/10.1016/j.surfcoat.2018.12.035.

4. Lei, Q., Li, Z., Han, L., Xiao, Z., Xiao, T.: Effect of aging time on the corrosion behavior of a Cu-Ni-Si alloy in 3.5 wt% NaCl solution, Corrosion, 72(5), 2016, 615–627. https://doi.org/10.5006/1884.

5. Zhang, Y., Tian, B., Volinsky, A.A. *et al.* Microstructure and Precipitate's Characterization of the Cu-Ni-Si-P Alloy. Journal of Materials Engineering and Performance, 25, 2016, 1336–1341. https://doi.org/10.1007/s11665-016-1987-6.

6. Li, J., Huang, G., Mi, X., Peng, L., Xie, H., Kang, Y.: Relationship between the microstructure and properties of a peak aged Cu–Ni–Co–Si alloy, Materials Science and Technology, 35(5), 2019, 606–614. https://doi.org/10.1080/02670836.2019.1576374.

7. Tan, Z.J., Da Ma, T., Zhang, L.M., Zhang, W.M., Jia, R.G., Cao, D.D., Ji, H.: Relationship between Corrosion Resistance and Microstructure of Copper-Nickel Alloy Pipes in Marine Engineering, Materials Science Forum, 2019, 389–397. https://doi.org/10.4028/www.scientific.net/MSF.944.389.

8. Nwaeju, C.C., Edoziuno, F.O., Adediran, A.A., Nnuka, E.E., Adesina, O.S.: Structural and properties evolution of copper – nickel (Cu – Ni) alloys : a review of the effects of alloying materials, Materiaux & Techniques, 109(2), 2021, 204. https://doi.org/10.1051/MATTECH/2021022.

9. Nwaeju, C.C., Edoziuno, F.O., Nnuka, E.E.: Predictive modeling and statistical analysis of mechanical properties of heat treated Cu-10 % Ni alloy using response surface methodology, Materials Today: Proceedings, 56, 2021, 2371-2382, https://doi.org/10.1016/j.matpr.2021.12.167.

10. William, D.N.J.: *Metallurgy of copper based alloys*, Copper Development Association, McLean, 2010, https://www.copper.org/resources/properties/703_5.

11. Nguyen, D.N., Hoang, A.T., Pham, X.D., Sai, M.T., Chau, M.Q., Pham, V.V.: Effect of Sn component on properties and microstructure Cu-Ni-Sn alloys, Journal of Teknology. 80(6), 2018, 43–51. https://doi.org/10.11113/jt.v80.11867.

12. Freudenberger, J., Warlimont, H.: *Copper and Copper Alloys*, in: Martienssen, W., Warlimont, H. (Eds.), Springer Handbook of Materials Data, Springer, Cham, 2018, 293–301. https://doi.org/10.1007/978-3-319-69743-7_12.

13. Jeong, Y.B., Jo, H.R., Kim, J.T., Hong, S.H., Kim, K.B.: A study on the micro-evolution of mechanical property and microstructures in (Cu-30Fe)-2X alloys with the addition of minor alloying elements, Journal of Alloys and Compounds, 786, 2019, 341–345. https://doi.org/10.1016/j.jallcom.2019.01.169.

14. Li, J., Huang, G., Mi, X., Peng, L., Xie, H., Kang, Y.: Effect of Ni/Si mass ratio and thermomechanical treatment on the microstructure and properties of Cu-Ni-Si alloys, Materials, 12, 2019, 2076. https://doi.org/10.3390/ma12132076.

15. Yi, J., Jia, Y., Zhao, Y., Xiao, Z., He, K., Wang, Q., Wang, M., Li, Z.: Precipitation behavior of Cu-3.0 Ni-0.72 Si alloy, Acta Materialia, 166, 2019, 261–270. https://doi.org/10.1016/j.actamat.2018.12.047.

16. Obayi, C.S.: Grain Size Evolution and Mechanical Properties of Thermomechanically Pure Iron Biodegradable Medical Implant Application, Nigerian Journal of Technology, 38, 2019, 804–812. https://doi.org/http://dx.doi.org/10.4314/njt.v38i3.37.

17. Estrin, Y., Vinogradov, T.: Extreme grain refinement by severe plastic deformation: A wealth of challenging science, Acta Materialia, 61, 2013, 782–817. https://doi.org/10.1016/j.actamat.2012.10.038.

18. Bai, X., Zhao, Y., Ma, J., Liu, Y., Wang, Q.: Grain-Size Distribution Effects on the Attenuation of Laser-Generated Ultrasound in α-Titanium Alloy, Materials, *12*(1), 2019, 102, https://doi.org/10.3390/ma12010102.

19. Zeng, F., Agnew, S.R., Raeisinia, B., Myneni, G.R.: Ultrasonic attenuation due to grain boundary scattering in pure

niobium, Journal of Nondestructive Evaluation 29, 2010, 93–103, https://doi.org/10.1007/s10921-010-0068-2.
20. Hall, E.O.: The deformation and ageing of mild steel: III discussion of results, Proceedings of Physics Society: Section B, 64, 1951, 747.
https://doi.org/10.1088/0370-1301/64/9/303.
21. Chapetti, M.D., Miyata, H., Tagawa, T., Miyata, T., Fujioka, M.: Fatigue strength of ultra-fine grained steels, Materials Science and Engineering A, 381, 2004, 331–336. https://doi.org/10.1016/j.msea.2004.04.055.
22. Uchic, M.D., Dimiduk, D.M., Florando, J.N., Nix, W.D.: Sample dimensions influence strength and crystal plasticity, Science, 305, 2004, 986–989.
https://doi.org/10.1126/science.1098993.
23. Ji, M., Janik, V., Strangwood, M., Davis, C.: Effect of Grain Size Distribution on Recrystallisation Kinetics in a Fe-30Ni Model Alloy. In *Proceedings of the 6th International Conference on Recrystallization and Grain Growth (ReX&GG 2016)*, 2016, 153–158. https://doi.org/10.1007/978-3-319-48770-0_22.
24. Paredes, C., Paredes-orta, C.A., Mendiola-santibañez, J.D., Manriquez-Guerrero, F.: Method for Grain Size Determination in Carbon Steels Based on the Ultimate Opening Method for grain size determination in carbon steels based on the ultimate opening, Measurement, 133, 2018, 193-207,.
https://doi.org/10.1016/j.measurement.2018.09.068.
25. Wu, Z., Cheng, Y.F., Liu, L., Lv, W., Hu, W.: Effect of heat treatment on microstructure evolution and erosion-corrosion behavior of a nickel-aluminum bronze alloy in chloride solution, Corrosion Science, 98, 2015, 260–270. https://doi.org/10.1016/j.corsci.2015.05.037.
26. Ralston, K.D., Birbilis, N.: Effect of grain size on corrosion: a review, Corrosion, 66(7), 2010, 75005. https://doi.org/10.5006/1.3462912.
27. Petch, N.J.: The cleavage strength of polycrystals, Journal of Iron and Steel Institute, 174, 1953, 25-28.
28. Gollapudi, S.: Grain size distribution effects on the corrosion behaviour of materials, Corrosion Science, 62, 2012, 90–94.
https://doi.org/10.1016/j.corsci.2012.04.040.
29. Nie, F.L., Zheng, Y.F., Wei, S.C., Hu, C., Yang, G.: In vitro corrosion, cytotoxicity and hemocompatibility of bulk nanocrystalline pure iron, Biomedical Materials, 5, 2010, 65015. https://doi.org/10.1088/1748-6041/5/6/065015.
30. Li, J.C.M.: Mechanical grain growth in nanocrystalline copper, Physics Review Letters, 96, 2006, 215506.
https://doi.org/10.1103/PhysRevLett.96.215506.
31. Ralston, K.D., Birbilis, N., Davies, C.H.J.: Revealing the relationship between grain size and corrosion rate of metals, Scripta Materialia, 63, 2010, 1201–1204. https://doi.org/10.1016/j.scriptamat.2010.08.035.
32. Kus, E., Lee, Z., Nutt, S., Mansfeld, F.: A comparison of the corrosion behavior of nanocrystalline and conventional Al 5083 samples, ECS Transactions, 62(2), 2006, 152–161. https://doi.org/10.5006/1.3278260.
33. Brunner, J.G., Birbilis, N., Ralston, K.D., Virtanen, S.: Impact of ultrafine-grained microstructure on the corrosion of aluminium alloy AA2024, Corrosion Science, 57, 2012, 209–214. https://doi.org/10.1016/j.corsci.2011.12.016.
34. Peregrina-Barreto, H.,Terol-Villalobos, I.R., Rangel-Magdaleno, J.J., Herrera-Navarro, A.M., Morales-Hernández, L.A., Manríquez-Guerrero, F.: Automatic grain size determination in microstructures using image processing, Measurement, 46, 2013, 249–258.
https://doi.org/10.1016/j.measurement.2012.06.012.
35. Edoziuno, F.O., Adediran, A.A., Odoni, B.U., Nwaeju, C.C., Adesina, O.S., Oki, M.: Influence of wormin mebendazole on the corrosion of mild steel in 1.0M sulphuric acid, Results in Engineering, 9, 2021, 100192.
https://doi.org/10.1016/j.rineng.2020.100192.
36. Barsoukov, E., MacDonald, J.R.: *Impedance Spectroscopy Theory, Experiment, and, Applications*, 2nd Ed., Hoboken, NJ John Wiley &Sons, 2005.
37. Ilangovan, S.: Study of microstructure, hardness and wear properties of sand cast Cu-4Ni-6Sn bronze alloy, Journal of Engineering, Science and Technology, 10(4), 2015, 526–532.
38. Lei, Q., Li, S., Zhu, J., Xiao, Z., Zhang, F., Li, Z.: Microstructural evolution, phase transition, and physics properties of a high strength Cu–Ni–Si–Al alloy, Materials Characterization, 147, 2019, 315–323.
https://doi.org/10.1016/j.matchar.2018.11.018.
39. Wallinder, I.O., Zhang, X., Goidanich, S., Le Bozec, N., Herting, G., Leygraf, C.: Corrosion and runoff rates of Cu and three Cu-alloys in marine environments with increasing chloride deposition rate, Science of the Total Environment, 472, 2014, 681–694.
https://doi.org/10.1016/j.scitotenv.2013.11.080.
40. Nwaeju, C.C., Edoziuno, F.O., Adediran, A.A., Tuaweri, T.J., Kumar, M.S.: Grain characteristics and mechanical properties of as-cast Cu-10 % Al alloy : Effects of alloying additions, Results in Engineering, 12, 2021, 100295. https://doi.org/10.1016/j.rineng.2021.100295.
41. Luo, Y., Deng, Y., Guan, L., Ye, L., Guo, X., Luo, A.: Effect of grain size and crystal orientation on the corrosion behavior of as-extruded Mg-6Gd-2Y-0.2Zr alloy, Corrosion Science, 164, 2020, 108338.
https://doi.org/10.1016/j.corsci.2019.108338.
42. Soltani, H., Ngomesse, F., Reinhart, G., Benoudia, M.C., Zahzouh, M., Nguyen-Thi, H.: Impact of gravity on directional solidification of refined Al-20wt.%Cu alloy investigated by in situ X-radiography, Journal of Alloys and Compound, 862, 2021, 158028, https://doi.org/10.1016/j.jallcom.2020.158028.
43. Nady, H., El-Rabiei, M.M., Abd El-Hafez, G.M. : Electrochemical Stability of Cu–10Al–10Zn, Cu–10Al–10Ni, and Cu–10Ni–10Zn Ternary Alloys in Simulated Physiological Solutions. *Journal of Bio- and Tribo- Corrosion*, 2(28), 2016,1-12. https://doi.org/10.1007/s40735-016-0058-8.
44. Ismail, K.M., Fathi, A.M., Badawy, W.A.: The influence of Ni content on the stability of copper – nickel alloys in alkaline sulphate solutions, Journal of Applied Electrochemistry, 34, 2004, 823–831.
https://doi.org/10.1023/B:JACH.0000035612.66363.a3.